Insight into Mechanical Properties and Strain-induced Crystallisation of Epoxidized Natural Rubber Filled with Various Silanized Halloysite Nanotubes

Abdulhakim Masa[a] , *Nabil Hayeemasae [b]**

[a]Prince of Songkla University, International College, Rubber Engineering & Technology Program, 90110, Hat Yai, Songkhla, Thailand.
[b]Prince of Songkla University, Faculty of Science and Technology, Department of Rubber Technology and Polymer Science, Pattani Campus, 94000, Pattani, Thailand.

Natural rubber (NR) and halloysite nanotube (HNT) composites are known to perform poorly due to polarity differences between the two components. As such, many extant studies have attempted to increase their compatibility. Therefore, this study introduced epoxidized natural rubber (ENR) together with silane coupling agents into the composite to ensure rubber-filler interactions. Four different silanes namely bis-[(triethoxysilyl)propyl] disulphide (TESPD), bis[(triethoxysilyl)propyl] tetrasulfide (TESPT), triethoxyvinylsilane (VTEO), and 3-mercaptopropyl-di(tridecan-1-oxy-13-penta(ethyleneoxide)) ethoxysilane (VPSi-363) were used. Fourier-transform infrared (FTIR) spectroscopy of the composite confirmed the formation of hydrogen bonds between the silane as the peak of Si-O shifted to higher wavenumbers; i.e., 1080 cm⁻¹ to 1042 cm⁻¹. Silane was also found to improve the tensile strength, modulus and tear strength regardless of functionality. This was further supported by the findings of the Payne effect. As for strain-induced crystallisation (SIC), the stress-strain curves agreed well with the development of crystallinity observed during synchrotron wide-angle X-ray scattering analysis.

Keywords: *Epoxidized natural rubber, Halloysite nanotubes, Silane coupling agent, Mechanical properties, Wide-angle X-ray scattering.*

1. Introduction

Rubber nanocomposites rely heavily on the characteristics of the rubbers and fillers[1], especially the polarity difference between those two phases. Apart from that, other factors of the filler, such as aspect ratio, degree of dispersion, and alignment; are also integral[2]. Various types of rubber nanocomposites are made from components that are dissimilar in nature. Halloysite Nanotubes (HNT) filled Natural Rubber (NR) composite is an example of an incompatible system simply because NR is classified as a non-polar rubber while HNT are not. As the surface chemistry of HNT is toward polarity due to the presence of aluminum, silicon, hydrogen, and oxygen[3], identifying an appropriate technique for addressing this downside is of keen attraction to researchers. As such, modified rubber has recently been used as a matrix in rubber/HNT composites. Hayeemasae et al.[4] discovered very interesting mechanical properties when epoxidized natural rubber was prepared as a matrix and filled with HNT. Paran et al.[5] also proposed the method to improve the properties of HNT composite by grafting HNT onto carboxylated nitrile rubber. As such, the findings of these studies make it clear that improved composite performance can be attained by substituting the polarity of the rubber matrix. Therefore, this study focused on transforming a non-polar NR into a polar NR. NR was first modified into an epoxidized natural rubber (ENR) and further applied as a matrix to ensure HNT–rubber compatibility. Although the

performance of this solution is well reported[4,6], it was still unsatisfactory as HNT characteristics could themselves be to blame; particularly the interfacial filler–matrix adhesion. This includes the use of silane coupling agents[7], modifying the compounding methods[8], and using compatibilizers[9].

Silane coupling agents have been widely employed and investigated over decades. As such, the application of silane is known to have practical relevance. Furthermore, the mechanism behind such improvement of the composites has also been well-recognised. Various silane coupling agents have been grafted onto HNT when preparing polymer composites. Yuan et al.[10] modified HNT by grafting it with organosilane (3-aminopropyl) triethoxysilane (APTES) and proposed a plausible reaction mechanism. They observed that the modification introduced not only the direct grafting of APTES onto the surface hydroxyl groups, but also oligomerisation as the hydrolysed APTES and the post-grafted APTES condensed to form a cross-linked structure. Evacuation pre-treatment was also found to considerably improve the loading of hydrolysed APTES into the lumen of HNT and increase the grafting ratio. Other types of silane coupling agents; namely γ-methacryloxypropyl trimethoxysilane (γ-MPS); have also been grafted on HNT to increase the interfacial adhesion of ethylene propylene diene rubber (EPDM) composites[11]. The grafting reaction was done in an ethanol medium while Fourier-transform infrared (FTIR) spectroscopy and thermogravimetric analysis (TGA) were implemented to verify grafting efficiency. The results

*e-mail: nabil.h@psu.ac.th

demonstrated that γ-MPS had partly perforated into the HNT and interacted with the Si-O groups on the surface of the HNT which enhanced the tensile strength of the EPDM/HNT nanocomposite.

Therefore, the purpose of this study was to use silane-treated HNT in the ENR matrix to improve the overall properties of the composites. It was hypothesised that interfacial adhesion between ENR and HNT may be improved as the epoxide group of the ENR ensures the interactions between rubber and HNT. This was anticipated to enhance the compatibility and facilitate homogeneous distribution within the composite resulting in enhanced reinforcing efficiency in HNT-filled NR composites. This study also proposed specific techniques for rating the reinforcing efficiency of the composites; such as dynamic property, mechanical properties, and strain-induced crystallisation (SIC). The latter is attractive as not many studies have investigated it. However, this can only be related to specific types of rubber, such as NR[12-14]. This is because NR has a very long chain whose arrangement and orientation facilitate crystallisation while stretching[15]. This potential to crystallise while stretching is simply due to the high regularity of NR molecular structure, which is almost 100% cis-1,4-polyisoprene[16].

Many NR-based studies have been performed with in situ deformation and in situ X-ray diffraction techniques[16-18]. Faster but limited development in crystallinity was observed in samples with higher crosslink density. SIC-based studies provide an alternative explanation regarding the onset of strain when rubber chains are crystallised. It was observed that the onset of strain in SIC always reduced after the addition of the filler[19]. However, different fillers may affect the formation of rubber-filler interaction and reactions differently[20,21] as they can either increase or decrease SIC depending on the chemical crosslink density of the NR matrix. As such, this study investigated correlations between rubber reinforcement and SIC in composites filled with various silane coupling agents. It was hypothesised that rubber-filler interactions may expedite the crystallisation process at certain network chain densities. As such, this study presents a corresponding wide-angle X-ray scattering and tensile measurement of silanized HNT-filled ENR composites.

To date, extant studies have not performed detailed investigations of the correlations between the mechanical properties and SIC in rubber composites. The use of silanized HNT filled ENR composites requires high mixing temperatures to obtain effective silanization. The results obtained in this study provide a scientific understanding of how silanized HNT affects the overall properties of ENR/HNT composites as well as useful information on producing ENR/HNT composites-based rubber products.

2. Experimental Set-up

2.1. Materials

High ammonia centrifuged latex (HA) with a 60% dry rubber content (DRC) was utilised to synthesise the ENR. This HA was centrifuged and provided by Chalong Latex Industry Co., Ltd., Songkhla, Thailand. To synthesise the ENR, teric N30 was used as the non-ionic surfactant while formic acid and hydrogen peroxide were used for the performic acid

reaction. These chemicals were acquired from Sigma Aldrich (Thailand) Co. Ltd., Bangkok, Thailand. The HNT was mined and provided by Imerys Ceramics Limited, Matauri Bay, New Zealand. HNT consist of the following components: 49.5 wt.% silicon dioxide (SiO_2), 35.5 wt.% aluminium oxide (Al_2O_3), 0.29 wt.% ferric oxide (Fe_2O_3), and 0.09 wt.% titanium dioxide (TiO_2) as well as traces of calcium oxide (CaO), magnesium oxide (MgO), potassium oxide (K_2O), and sodium oxide (Na_2O). The silane coupling agents used in this study; namely (bis-[(triethoxysilyl)propyl]disulphide (TESPD; MW = 474.82 g/mol), (bis-(triethoxysilylpropyl) tetrasulfide (TESPT; MW = 538.95 g/mol), 3-mercaptopropyl-di(tridecan-1-oxy-13-penta(ethyleneoxide))ethoxysilane (VPSi-363; MW = 987.50 g/mol), and triethoxyvinylsilane (VTEO; MW = 190.31 g/mol); were supplied by Evonik Industries, Essen, Germany. The chemical structures of all silanes are illustrated in Figure 1. Stearic acid was supplied by Imperial Industrial Chemicals (Thailand) Co., Ltd., Bangkok, Thailand. ZnO was sourced from Global Chemical Co., Ltd., Samut Prakan, Thailand, while N-cyclohexyl-2-benzothiazole sulphenamide was obtained from Flexsys America L.P., Akron, Ohio, USA, and soluble sulphur was purchased from Siam Chemical Industry Co., Ltd., Samut Prakan, Thailand.

2.2. Synthesis of epoxidized natural rubber

Firstly, HA latex was diluted to gain a DRC of 15%. Next, 1 phr of 10% teric N30; a non-ionic stabiliser; was added and kept stirring for 30 minutes at room temperature. This was to evaporate the ammonia dispersed in HA latex. Epoxidation was carried out using performic acid (formic acid and hydrogen peroxide) at 50 °C in a 10 L glass vessel at a stirring rate of 30 rpm. The reaction time was set carefully to gain ENR with 20 mol% epoxide. The resulting ENR was coagulated with methanol followed by washing with water. Finally, it was dried in a vacuum oven at 50 °C before use.

2.3. Preparation of silanized HNT-Filled ENR composites

Table 1 depicts the preparation of the ENR/HNT composites filled with unsilanized and silanized HNT. An individual silane, ENR with 20 mol% epoxide (ENR 20), was compounded with 5 phr of HNT and the other ingredients except for the curatives (N-cyclohexylbenzothiazole-2-sulphenamide (CBS) and sulphur) in a Brabender® Plasti-Corder® Lab-Station (Brabender GmbH & Co. KG, Duisburg, Germany). The optimum properties observed from our previous
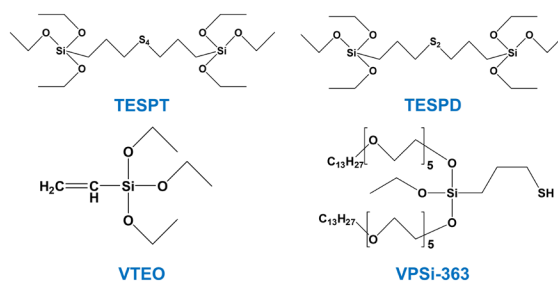

Figure 1. Chemical structures of TESPT, TESPT, VTEO and VPSi-363.

Insight into Mechanical Properties and Strain-induced Crystallisation of Epoxidized Natural Rubber Filled
with Various Silanized Halloysite Nanotubes

3

Table 1. Formulation of silane treated HNT filled NR composites.

Raw Material	Amount (phr)
ENR 20	100.0
Stearic acid	1.0
Zinc oxide	5.0
HNT *	5.0
Silane coupling agent*	0.001 mole alkoxy group equivalent
CBS	2.0
Sulfur	2.0

Remark: *Different types of silane coupling agents namely TESPD, TESPT, VTEO, and VPSi-363.

studies were used to fix the mol% of epoxide and HNT[4,22]. The composite filled with unsilanized HNT was labelled "ENR20" while the silanized HNT-filled composites; namely TESPD, TESPT, VTEO, and VPSi-363; were labelled using their abbreviations. The mixing temperature of 60 °C was reached before finally dumping the temperature at 110 °C with a rotor speed of 60 rpm. The resulting compound was then sheeted on a two-roll mill while the curing agents were added. Finally, the curing characteristics of the individually silanized HNT filled compounds were tested.

2.4. Measurement of curing characteristics

A Rheo-Line Mini-MDR Lite (Prescott Instruments Ltd., Tewkesbury, UK) moving die rheometer was used to measure the curing properties of the composites according to ASTM D5289[23]. The running temperature was set at 150 °C and data; such as torque, scorch time (t_{s2}), and curing time (t_{c90}); were recorded. As seen in Equation 1, the t_{s2} and t_{c90} were used to calculate the curing rate index (CRI) as follows:

$$CRI = \frac{100}{t_{c90} - t_{s2}} \qquad (1)$$

2.5. Fourier transform infrared-spectroscopic analysis (FT-IR)

Fourier-transform infrared (FTIR) spectroscopy was conducted using a Bruker® Tensor 27 FTIR Spectrometer (Billerica, Massachusetts, USA) to confirm the functional changes of ENR composites filled with unsilanized and silanized HNT. The spectra display in transmission mode with a 4 cm⁻¹ resolution over 4000 to 550 cm⁻¹.

2.6. X-ray diffraction analysis (XRD)

An x-ray diffraction (XRD) analysis of ENR composites filled with unsilanized and silanized HNT was conducted using a Philips® X'Pert-MPD diffractometer (Eindhoven, The Netherlands) with CuKα radiation (λ = 0.154 nm) at 40 kV and a current of 30 mA. The diffraction patterns were scanned at diffraction angles of 2θ° from 5° to 30° with a step size of 0.05° and 3° per minute scan speed. Bragg's equation was then used to estimate the d-spacing of HNT layers in the particles.

2.7. Measurement of tensile properties, tear strength and hardness

The tensile properties were determined according to ASTM D412[24]. The dimensions of the sample were based on a "Die C" dumbbell shape. The test was done using a Tinius Olsen® H10KS universal testing machine (Tinius Olsen Ltd., Surrey, UK) at a crosshead speed of 500 mm/min. The recorded results were the stresses at 100% (M100) and 300% (M300) strains, elongation at break and tensile strength. The tear strength of the respective composites was done using a similar machine and crosshead speed according to ASTM D624[25]. A type C (right angle) test specimen was selected for the experiment. The final measurement of the samples, the hardness property, was tested according to ASTM D2240[26] using a Shore A manual durometer.

2.8. Scanning electron microscopy

The morphology of ENR composites filled with unsilanized and silanized HNT was screened from the tensile fractured surfaces. The image was captured using a FEI Quanta™ 400 FEG scanning electron microscope (SEM; Thermo Fisher Scientific, Waltham, Massachusetts, USA). As such, the specimen was coated with a layer of gold/palladium to remove the charges built-up during imaging.

2.9. Dynamic properties

A MonTech® D-RPA 3000 dynamic rubber process analyser (RPA; MonTech Werkstoffprüfmaschinen GmbH, Buchen, Germany) was used to analyse the dynamic properties of the composites. The test samples were first vulcanised at 150 °C referred to the t_{c90} tested by the same RPA. The samples were then cooled to 60 °C. At this time, the strain was varied from 0.5% to 90% at a fixed frequency of 10Hz to ascertain the storage modulus (G') at various applied strains in the composites. This raw G' record was additionally used to observe filler–filler interactions via the so-called Payne effect. Equation 2 was used to calculate the Payne effect:

$$Payne\ effect\ = G'_i - G'_f \qquad (2)$$

where G'_i and G'_f were the G' at strains of 0.5% and 90%, consecutively. The larger the Payne effect, the higher the filler–filler interactions.

2.10. Wide-angle x-ray scattering

The strain-induced crystallisation (SIC) of the composite was correlated with the stress-strain curves of the composite. The SIC and other related findings were obtained using synchrotron wide-angle X-ray scattering (WAXS) analysis. The Beamline 1.3W at the Siam Photon Laboratory, Synchrotron Light Research Institute (SLRI), Nakhon Ratchasima, Thailand was used to experiment. The gap between the sample and the detector was 115.34 mm, evaluated using a wavelength of 0.138 nm. A Rayonix© SX165 charge-coupled device (CCD)-based X-ray detector (Evanston, Illinois, USA), with an active area of 165 mm in diameter, was used to detect the WAXS profile. The scattering angle was calibrated using 4-bromobenzoic acid as a standard material.

Before the test, the "Die C" shaped dumbbell specimen was held on the grips of a stretching equipment. The sample was pulled at a crosshead speed of 50 mm/min at a fixed strain before it was relaxed in the stretch condition for 30 seconds. The WAXS was recorded before stretching was recommenced until the next predetermined strain and

the characterisation was complete. Equation 3 was used to calculate the degree of crystallinity (X_c) using the data acquired from the WAXS profiles:

$$\text{Degree of crystallinity } (X_c) \ = \left(\frac{A_c}{A_c + A_a}\right) \times 100 \qquad (3)$$

where A_c is and A_a are the areas under the crystalline peak of interest and the amorphous halo, respectively.

As seen in Equation 4, the orientation parameter (OP) was determined using the Hermann equation as follows:

$$\text{OP} \ = \frac{3[\cos^2\phi] - 1}{2} \qquad (4)$$

where φ is the azimuthal angle concerned with the direction of strain. As seen in Equation 5, the mean value of $\cos^2 \varphi$ was calculated as follows:

$$[\cos^2\phi] = \frac{\int_0^\pi I_c(\phi) \cdot \cos^2\phi \cdot \sin\phi \cdot d\phi}{\int_0^\pi I_c(\phi) \cdot \sin\phi \cdot d\phi} \qquad (5)$$

where $I_c(\varphi)$ is the scattering intensity of the crystal at φ. $I_c(\varphi)$ was normalised by subtracting the minimum scattering intensity of the amorphous constituent of the earlier WAXS intensity[27,28].

3. Results and Discussion

3.1. FT-IR analysis

Figure 2 shows the Fourier-transform infrared (FTIR) spectra of epoxidized natural rubber (ENR) composites filled with unsilanized and silanized halloysite nanotubes (HNT). The spectra showed the peak of the hydrocarbon structure, i.e., the stretching vibration of the C=C bond, the bending vibration of the CH_2 and CH_3 groups, and the out of plane deformation of the =C-H group which was obvious at 1662 cm^{-1}, 1448 cm^{-1}, 1375 cm^{-1}, and 837 cm^{-1}, consecutively. The peak absorptions observed at 873 cm^{-1} and 1250 cm^{-1} related to the epoxide ring created on the NR backbone. The peak at

3400 cm^{-1} was the stretching vibration of hydroxyl groups indicating the opening reaction of the acid-catalysed ring of the epoxy group to form the alcohol hydroxyl[29]. The absorption bands at 3694 cm^{-1} and 3622 cm^{-1} are specifically appointed to the vibrations of hydroxyl groups, which are the stretching vibrations of the inner surface hydroxyl groups and the outer hydroxyls groups[30]. It is noteworthy that the peak in the 1100 cm^{-1} to 1020 cm^{-1} region is ascribed to the absorption of the stretching vibration of the Si-O bond, which shifted from 1042 cm^{-1} to 1036 cm^{-1} and from 1076 cm^{-1} to around 1081 cm^{-1}. This shifting indicates that a change in the environment surrounding the Si-O bond due to the formation of hydrogen bonds[11]. Such formations are responsible for enhancing rubber-filler interactions in the system. This will be discussed in later sections.

3.2. X-ray diffraction analysis

X-ray diffraction (XRD) analysis also confirmed an improvement in rubber-filler interactions. As seen in Figure 3, the diffraction peak at 2θ of 12.05° (d is 7.33 Å) is related to the 001 plane. This basal reflection of HNT was presented due to the tubular structure, high degree of disorganisation, small crystal size, and interstratification of layers with various hydration conditions[31]. The introduction of silane to the composites changed crystal order especially in bis-[(triethoxysilyl)propyl] disulphide (TESPD) and bis[(triethoxysilyl) propyl] tetrasulfide (TESPT). A 2θ decrease was found at 8.48° corresponding to the 10.41 Å basal spacing. This 2θ reduction and distance gallery increase in the HNT may be ascribed to the intercalation of the HNT by the silane and the other materials[32]. The intercalation of silane into the lumen of HNT could induce more interactions between the hydroxyl groups inside the HNT lumen and silane which will result in more interactions in the rubber matrix.

3.3. Curing characteristics

The rheometric curves and corresponding outputs of ENR composites filled with unsilanized and silanized HNT are illustrated and listed in Figure 4 and Table 2,
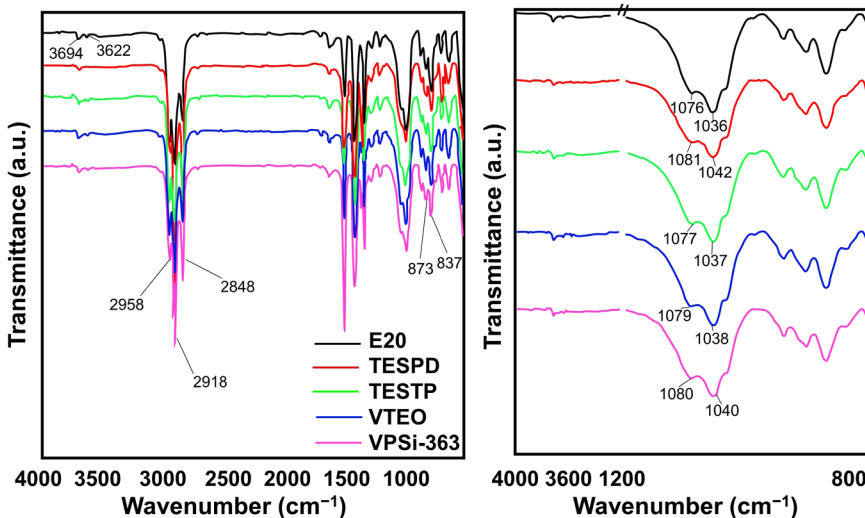

Figure 2. Infrared spectra of ENR composites filled with unsilanized and silanized HNT.

Insight into Mechanical Properties and Strain-induced Crystallisation of Epoxidized Natural Rubber Filled
with Various Silanized Halloysite Nanotubes

5

consecutively. The addition of silane coupling agents in the composites resulted in decreased scorch time (t_{s2}) and curing time (t_{c90}) as well as increased cure rate index than
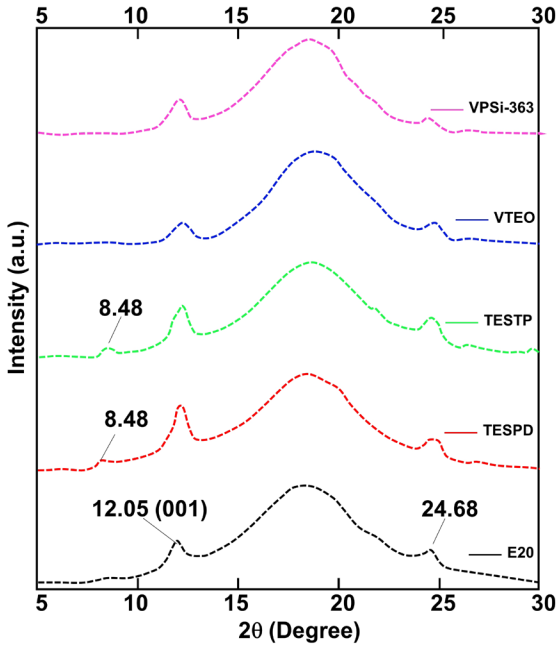

Figure 3. XRD scattering patterns of ENR composites filled with unsilanized and silanized HNT.
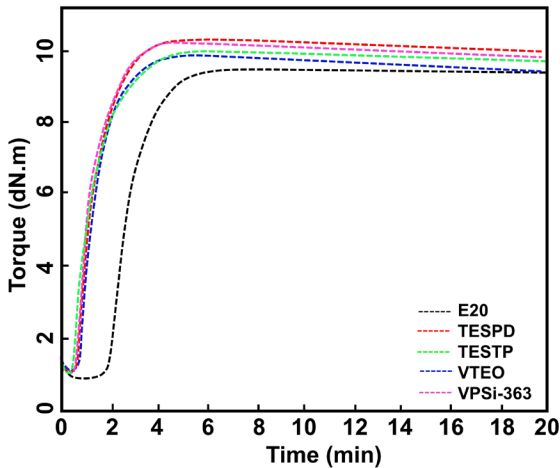

Figure 4. Rheometric curves of ENR composites filled with unsilanized and silanized HNT.

composites without silane. As such, it is evident that silanes change the vulcanisation process of rubber regardless of the type of silane used. As seen in the silane chemical structures depicted in Figure 1, the four investigated silanes have unique functionalities that could expedite the vulcanisation process of rubber. For instance, as TESPD, TESPT, and VPSi-363 contain reactive sulphur atoms in the molecule, they may accelerate the vulcanisation process by producing a reactive sulphurating agent that can crosslink with rubber molecules[31,33]. Furthermore, although the chemical structure of triethoxyvinylsilane (VTEO) differs as it does not contain sulphur atoms, it contains a vinyl backbone that enables it to form crosslinks through a C=C bond[33] and/or react with the sulphur atoms in the rubber ingredient. Therefore, silane reduces both the scorch time (t_{s2}) and curing time (t_{c90}) with differences in value arising from the affinity of such functionalities to form crosslinks during heating. Another probable reason might be the decreased tendency of silanes to adsorb the accelerator[22].

In unsilanized HNT, the silanol groups are still present and tend to form hydrogen bonds with the accelerator, which causes the accelerator to work slower. This is not happened to silanized HNT. Silanol groups were coupled with silanes during silanization. Therefore, there was no active sites left to interact with accelerator, making the accelerator perform well during vulcanisation. Silanes were also found to increase minimum torque (M_L). As the viscosity of the compound affects M_L, it is possible that the interaction affects the viscosity of the compound. Furthermore, composites filled with silanized HNT had slightly higher maximum torque (M_H) and delta torque ($M_H - M_L$) than their unsilanized counterparts. As such, an interaction may have taken place to cause an increase in these values after the introduction of a silane coupling agent[11]. Furthermore, the reliance of the chemical constituents on the chemical structures of the silanes may be another possible explanation as the sulphur atoms and vinyl group of these structures may influence the results.

3.4. Dynamic properties

Figure 5 presents the storage modulus (G') and the Payne effect of ENR composites filled with unsilanized and silanized HNT. Dynamic properties are another method of assessing possible interactions within a composite. At low strain, all the composites exhibited a similar trend. The G' was found to decrease slightly when strain was applied and dropped sharply at high strain, especially when subjected to more than 50% strain. This is common among viscoelastic materials due to the molecular stability of the rubber. The use of silane was found to provide higher G' at higher strains than in unsilanized samples. This alluded to the occurrence

Table 2. Scorch time, cure time, minimum torque, maximum torque, delta torque and cure rate index values of ENR composites in the presence of various silane coupling agents.

Sample	t_{s2} (min)	t_{c90} (min)	M_L (dN.m)	M_H (dN.m)	$M_H - M_L$ (dN.m)	CRI (min^{-1})
E20	2.20	4.70	0.85	9.44	8.59	40.00
TESPD	0.86	2.74	1.04	10.40	9.36	53.19
TESPT	0.79	2.60	1.10	10.18	9.08	55.25
VTEO	0.96	3.01	1.17	9.78	8.61	48.78
VPSi-363	0.69	2.66	1.16	10.38	9.22	50.76

of interactions between silanized HNT and ENR that give rise to greater elastic response. There are two factors that determine an increase in G': better interfacial adhesion of HNT eased by silane coupling agent and improved interactions between polarity matching HNT and ENR.

The mechanisms illustrated in Figure 6 clearly show interactions between ENR and silanized HNT. These mechanisms depended on the ambient temperature: (1) the silanization or silane to HNT reaction; (2) the coupling or silane to ENR reaction; and (3) ENR crosslinking originating from vinyl group (VTEO) or active sulphur let by the polysulfide-based silanes; i.e., TESPT, TESPD, and VPSi-363. In the third temperature-dependent mechanism, the observed reactions differed according to the active sites of
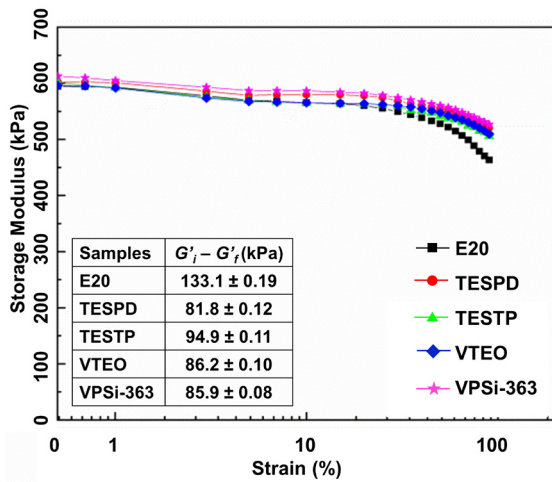

Figure 5. Strain dependence of storage modulus and delta G' for ENR composites filled with unsilanized and silanized HNT.

the silane. In sulphide-based silanes; such as TESPT, TESPD, and VPSi-363; crosslinks were formed via the sulphur that was released at high temperature. However, in vinyl-based silane; such as VTEO; crosslinks occurred via C=C bonds and the active radicals generated while mixing[33].

The Payne effect measures rubber–filler interactions in a composite. In this study, it was measured as the difference in G' between low and high strains. The results of the Payne effect indicated decreased rubber–filler interactions. For instance, the Payne effect of composites filled with unsilanized HNT was 133.1 kPa. This reduced to 81.85 kPa, 94.94 kPa, 86.23 kPa, and 85.89 kPa for TESPD, TESPT, VTEO, and VPSi-363, respectively, when silanes were incorporated. This reduction can be ascribed to the diminishing efficiency of filler-filler interactions by silane through the silanization process. According to the delta G' value, TESPD had the lowest value which indicated that it had the lowest filler-filler interactions in this system. As such, this suggests that TESPD is the best suited for ENR/HNT composites if the lowest Payne effect is a major concern.

3.5. Mechanical properties and morphologies

Figure 7 exhibits the stress–strain curves of ENR composites filled with unsilanized and silanized HNT. These stress–strain curves depict the occurrence of strain-induced crystallisation (SIC). A higher stress response was detected among composites filled with silanized HNT, regardless of the silane type. This suggests that the samples become stronger when using silanized HNT. Therefore, the improved compatibility of ENR with silanized HNT are responsible. The area under the stress–strain curve was also observed to verify the compatibility of the ENR and HNT. This stipulates the toughness of a rubber[34] as a wider area under the curve (AUC) corresponds to higher toughness. Composites with
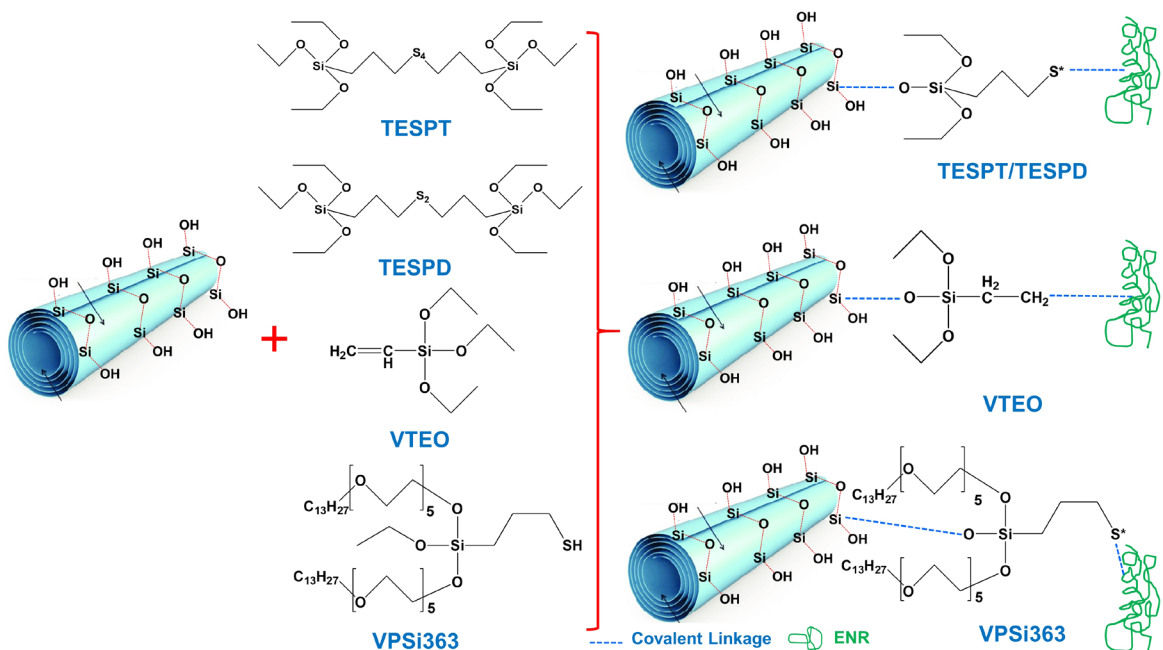

Figure 6. Possible interactions of ENR composites filled with various silanized HNT.

silanized HNT had a larger area under the stress–strain curve than their unsilanized counterparts and, thus, superior toughness. The shown curves are further stated in terms of crystallisation behaviour.

Table 3 lists mechanical properties, such as tensile properties, tear strength, and hardness of ENR composites filled with unsilanized and silanized HNT. Higher stress at strains of 100% (M100) and 300% (M300) were found for the ENR composites filled with silanized HNT. The TESPD was found to have the highest modulus. As previously mentioned, a sulphide-based accelerator could donate some of its sulphur during the vulcanisation process, thereby providing composites with extra crosslinks. However, although TESPT contains a higher amount of sulphur, it may not work well in this system. This is contradictory to the findings of a study by Kaewsakul et al.[33], where TESPT was found to have the highest performance due to the sulphur atoms available in its structure. However, Kaewsakul et al.[33] used NR, which contains more double bonds than the ENR used in this present study. As less concentrations of diene may require less sulphur to form crosslinks, TESPD seems to work well in this case.

Similar trends were also observed in terms of the hardness of the composites. The results matched a decrease in elongation at break of the composites well. This was because the filler-matrix interactions decreased the flexibility of the molecular chains. The resultant modulus trend matched the hardness observations well. The tensile strength (TS) and tear strength (Ts) of composites filled with unsilanized and silanized HNT also increased with the addition of silane regardless of the type of silane. TESPD had the highest increase in TS; from
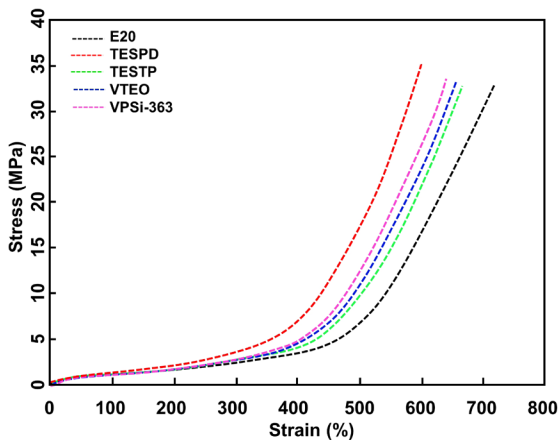

Figure 7. Stress-strain relationships of ENR composites filled with unsilanized and silanized HNT.

33.67 MPa to 35.09 MPa and then to 35.45 MPa while the Ts of the composites grew from 38.29 N/mm to 40.41 N/mm. As such, the use of silanized HNT evidently enhanced interfacial adhesion via certain chemical interaction/reaction of HNT. Evidence of such improvement has already been appeared in preceding sections of this present study. The SEM micrographs of composites with difference silane coupling agents are displayed in Figure 8. Sulphide-based silane composites; namely TESPD, TESPT, and VPSi-363; had pretty good dispersion, where clear tubular shapes of HNT scattered well in the matrix. This corresponded to better mechanical properties found in the previous explanation. However, such image was not seen for VTEO where the HNT seemed to be broken and agglomerated from one to another. This may have affected the tensile and tear strengths of the composite.

3.6. Wide-angle X-ray scattering

In the section regarding tensile properties, the stress–strain behaviour of the composites was aligned with SIC. As the nominal strain rate for tensile and SIC measurements differ; e.g., 0.42 s^{-1} and 0.042 s^{-1} for tensile test and WAXS, consecutively; a relationship was assembled for stress against crystallinity only. The previous sections have made it clear that the use of silanized HNT influences mechanical properties. The main factors have been discussed in the section regarding dynamic properties. The degree of crystallinity (Xc) as a function of applied strains is depicted in Figure 9. Crystallinity was evaluated from areas in the diffraction pattern for 200 and 120 plane reflections[35,36]. As expected, the Xc was found to increase with strain due to an orientation of molecular chains. While evaluating the Xc and stress development during tensile test (see Figure 7), it became obvious that the Xc agreed well with the stress. The tendency of the curves was also identical for certain silane types. As observed in the stress–strain curves, the stress increased with treatment time. This contributed to better rubber-fillers interactions, as previously discussed. Therefore, interacting/reacting points play a very important role in inducing crystallisation upon stretching. The schematic model presented in Figure 10 provides a further explanation.

As seen in the scheme, nothing occurred when the specimen was not deformed. At this point, the ENR matrix may be interacted HNT due to interfacial interactions resulting from the polar sites of HNT and ENR. However, when strain was given to the sample, crystallisation of the ENR was caused and increased together with the orientation of the HNT. HNT were oriented and constantly aligned to the deformed direction. This consistently took place regardless of whether unsilanized and silanized HNT was used. As other

Table 3. Tensile properties, tear strength and hardness of ENR composites filled with unsilanized and silanized HNT.

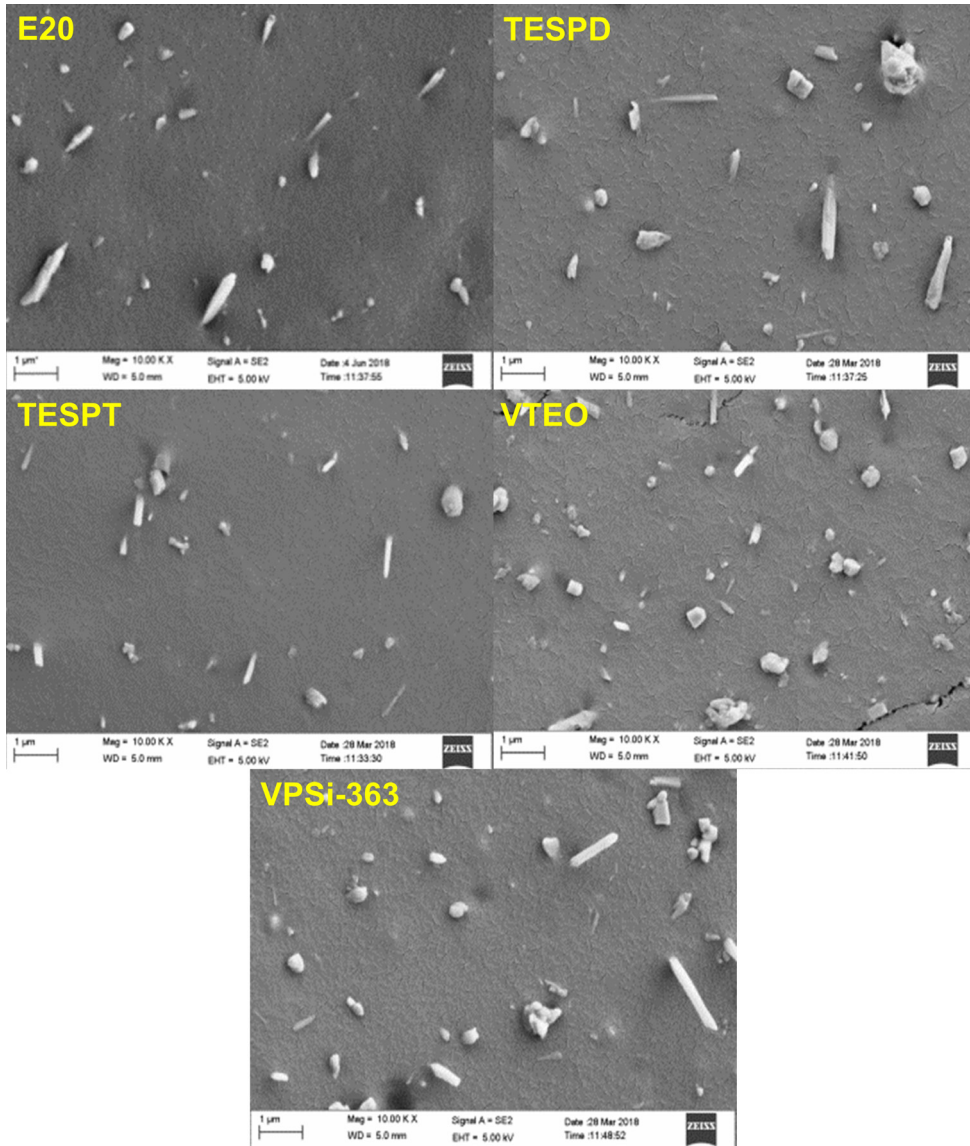| Sample	M100 (MPa)	M300 (MPa)	TS (MPa)	EB (%)	Ts (N/mm)	Hardness (Shore A)
E20	0.86 ± 0.03	2.25 ± 0.03	33.67 ± 1.61	717 ± 10	38.29 ± 0.94	39.3 ± 0.3
TESPD	0.94 ± 0.04	3.11 ± 0.18	35.09 ± 0.37	569 ± 32	40.31 ± 0.86	42.4 ± 0.4
TESPT	0.87 ± 0.02	2.58 ± 0.06	33.85 ± 0.62	657 ± 24	38.60 ± 0.44	41.2 ± 0.7
VTEO	0.91 ± 0.02	2.68 ± 0.01	34.05 ± 1.96	635 ± 09	38.69 ± 0.92	41.8 ± 0.5
VPSi-363	0.93 ± 0.02	2.78 ± 0.19	34.57 ± 1.27	629 ± 21	39.31 ± 1.04	42.1 ± 0.4

Figure 8. SEM photographs at 10,000× magnification of ENR composites filled with unsilanized and silanized HNT.
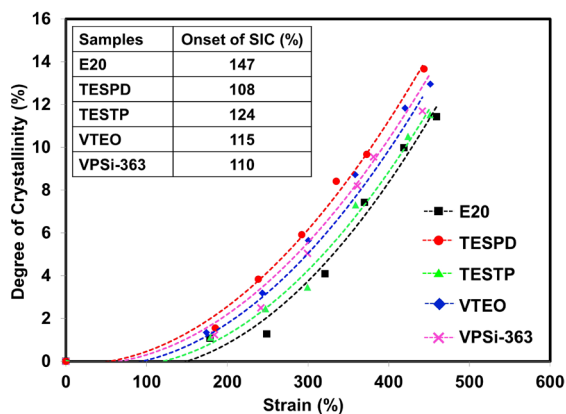

Figure 9. Degree of crystallinity as a function of applied strain and their corresponding onset of SIC of ENR composites filled with unsilanized and silanized HNT.

studies have also reported similar observations[21,37,38], this behaviour was common among filled composites. However, it is noteworthy that the crystallinity of the ENR matrix grew constantly due to the crystallisation of ENR and silanized HNT. Higher rubber–filler interactions, as demonstrated by a lower Payne effect, were responsible for this phenomenon. The presence of silanized HNT plays an important role in pulling the surrounding molecular chains. Therefore, an obvious increase in crystallisation was found at higher strains. This scheme provides a good explanation regarding the correlation between stress–strain behaviour and Xc.

The onset of strain during SIC was determined by intercepting a regression line for Xc against strain deformation (see the data inserted in Figure 9). The onset for SIC in composites filled with silanized HNT was found to be lower, regardless of silane type. TESPD has the slowest onset of SIC when using a silane. This corroborates well with the
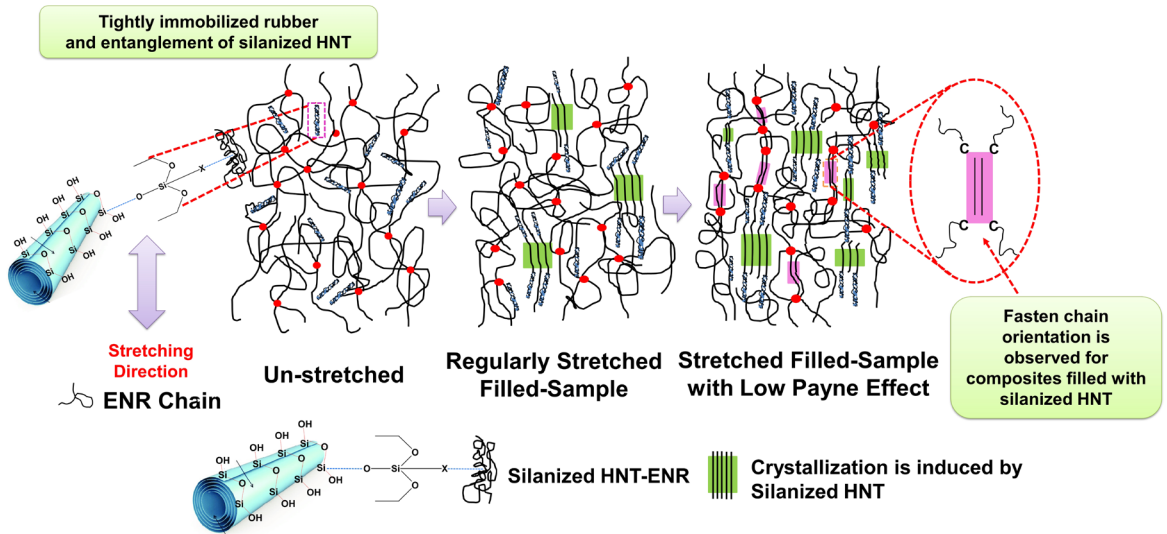
Insight into Mechanical Properties and Strain-induced Crystallisation of Epoxidized Natural Rubber Filled
with Various Silanized Halloysite Nanotubes

9

Figure 10. Schematic model representing the crystallization development of ENR composites filled with variously silanized HNT.

tensile and tear strengths of the composites. As such, the interaction that occurs in the presence of silanized HNT helps pulling the adjacent molecular chains and fastens the crystallisation process. The faster onset of SIC is common among filled composites. Poompradub et al.[20] found that orientational fluctuation increased when filler was included. However, the onset of SIC was depended on characteristics of filler. Ozbas et al.[37] differentiated the SIC of carbon black (CB) and graphene filled composites and observed that the onset of SIC taken place at obviously lower strains among graphene-filled NR samples than CB-filled NR, even at low loadings. Chenal et al.[21] further stated that the onset of SIC is determined by the strain amplification caused by the filler. Moreover, supplemental interactions in the rubber network are also accountable for either accelerating or slowing the crystallisation rate, depending on interaction/ reaction taking place in the system. The findings of both Ozbas et al.[37] and Candau et al.[38] further emphasised that rubber–filler interactions may expedite SIC. As such, it can be concluded that rubber-filler interactions occurred as the silanization and coupling reaction is clearly responsible for speeding up the crystallisation process of rubber. Therefore, the change in SIC was attributed to rubber–filler interactions.

The orientation and alignment of rubber molecular chain was evaluated using an orientation parameter (OP) which was computed using the Herman equation. Figure 11 shows the orientation parameter plotted as a function of strain. Completely oriented molecular chains have OP at 1[39]. In the present study, the OP of the composites was lower at low strains and grew with increasing strain, thereby confirming that stretching oriented the molecular chains. It was also observed that the OP value of all the composites grew concurrently with an increase in strain deformation. This was because more chain orientation occurred during stretching. TESPD had the highest OP value indicating that the molecular chains rearranged completely and most of the molecular chain orientation was found. This correspond well with the previously found Xc value and onset of SIC. Similar
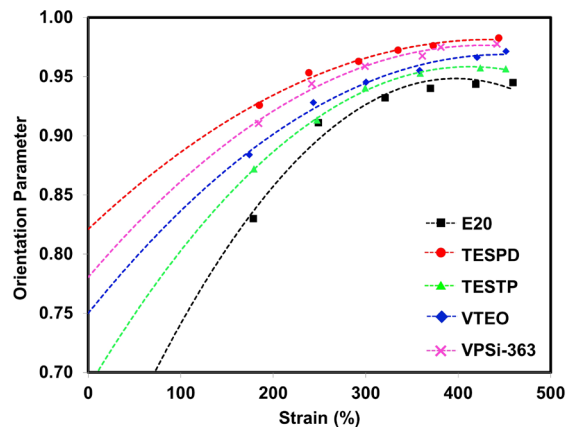

Figure 11. Orientation parameter as a function of applied strain of ENR composites filled with unsilanized and silanized HNT.

findings were also observed with other types of silane, which related to the previous WAXS profile.

4. Conclusions

Silane coupling agents were able to successfully enhance ENR/HNT composites. Using silanes has improved the modulus, tensile strength, and tear strength, regardless of their functionalities. This was due to the formation of hydrogen bonds between silane as confirmed by FTIR where the composites filled with TESPD-silanized HNT had the most optimum mechanical properties. This was ascribed to lower filler-filler interactions proved by the Payne effect. The strain-induced crystallisation (SIC) in the composites showed a significant change as the strain upturn was at an earlier strain during stretching. This indicated faster crystallisation due to better interfacial interactions within the composites. As such, based on the overall findings, the use of TESPD as a silane is highly recommended for producing composites

with an ENR matrix, enhancing filler-matrix compatibility, and increasing the strength of the composite vulcanizates. Furthermore, treating HNT with silane could be the solution to boosting ENR-HNT interactions, regardless of silane type. Silanes can also be used without a pre-treatment process as it can be added directly during mixing at a certain temperature, making it a practical solution.

5. Acknowledgments

6. References

1. Nguyen LT, Le Tran H, Mai PT, Duong VB, Nguyen L-TT, Nguyen HT. Poly (L-glutamic acid) via catalytic hydrogenation for the fabrication of carbon nanotube nanocomposites. Mater Res. 2021;24(1):e20200321. http://dx.doi.org/10.1590/1980-5373-mr-2020-0321.

2. Batista LA, da Cunha TH, Felisberto MD, Cetlin PR, Mazzer EM. Processing of an AA7050/Al hybrid composites reinforced with multiwalled carbon nanotubes. Mater Res. 2021;24:e20210077. http://dx.doi.org/10.1590/1980-5373-mr-2021-0077.

3. Price RR, Gaber BP, Lvov Y. In-vitro release characteristics of tetracycline HCl, khellin and nicotinamide adenine dineculeotide from halloysite; a cylindrical mineral. J Microencapsul. 2001;18:713-22. http://dx.doi.org/10.1080/02652040010019532.

4. Hayeemasae N, Waesateh K, Saiwari S, Ismail H, Othman N. Detailed investigation of the reinforcing effect of halloysite nanotubes-filled epoxidized natural rubber. Polym Bull. 2021;78:7147-66. http://dx.doi.org/10.1007/s00289-020-03461-4.

5. Paran SMR, Naderi G, Mosallanezhad H, Movahedifar E, Formela K, Saeb MR. Microstructure and mechanical properties of carboxylated nitrile butadiene rubber/epoxy/XNBR-grafted halloysite nanotubes nanocomposites. Polymers (Basel). 2020;12:1192. http://dx.doi.org/10.3390/polym12051192.

6. Surya I, Waesateh K, Masa A, Hayeemasae N. Selectively etched halloysite nanotubes as performance booster of epoxidized natural rubber composites. Polymers (Basel). 2021;13:3536. http://dx.doi.org/10.3390/polym13203536.

7. Paszkiewicz S, Irska I, Taraghi I, Piesowicz E, Sieminski J, Zawisza K, et al. Halloysite nanotubes and silane-treated alumina trihydrate hybrid flame retardant system for high-performance cable insulation. Polymers (Basel). 2021;13:2134. http://dx.doi.org/10.3390/polym13132134.

8. Paran S, Naderi G, Ghoreishy M. XNBR-grafted halloysite nanotube core-shell as a potential compatibilizer for immiscible polymer systems. Appl Surf Sci. 2016;382:63-72. http://dx.doi.org/10.1016/j.apsusc.2016.04.087.

9. Du M, Guo B, Lei Y, Liu M, Jia D. Carboxylated butadiene–styrene rubber/halloysite nanotube nanocomposites: interfacial interaction and performance. Polymer (Guildf). 2008;49:4871-6. http://dx.doi.org/10.1016/j.polymer.2008.08.042.

10. Yuan P, Southon PD, Liu Z, Green ME, Hook JM, Antill SJ, et al. Functionalization of halloysite clay nanotubes by grafting with γ-aminopropyltriethoxysilane. J Phys Chem C. 2008;112:15742-51. http://dx.doi.org/10.1021/jp805657t.

11. Pasbakhsh P, Ismail H, Fauzi MA, Bakar AA. EPDM/modified halloysite nanocomposites. Appl Clay Sci. 2010;48:405-13. http://dx.doi.org/10.1016/j.clay.2010.01.015.

12. Trabelsi S, Albouy PA, Rault J. Stress-induced crystallization properties of natural and synthetic cis-polyisoprene. Rubber Chem Technol. 2004;77:303-16. http://dx.doi.org/10.5254/1.3547825.

13. Toki S, Hsiao BS. Nature of strain-induced structures in natural and synthetic rubbers under stretching. Macromolecules. 2003;36:5915-7. http://dx.doi.org/10.1021/ma034729e.

14. Candau N, Chazeau L, Chenal JM, Gauthier C, Munch E. A comparison of the abilities of natural rubber (NR) and synthetic polyisoprene cis-1, 4 rubber (IR) to crystallize under strain at high strain rates. Phys Chem Chem Phys. 2016;18:3472-81. http://dx.doi.org/10.1039/C5CP06383C.

15. Lake GJ. Fatigue and fracture of elastomers. Rubber Chem Technol. 1995;68:435-60. http://dx.doi.org/10.5254/1.3538750.

16. Huneau B. Strain-induced crystallization of natural rubber: a review of X-ray diffraction investigations. Rubber Chem Technol. 2011;84:425-52. http://dx.doi.org/10.5254/1.3601131.

17. Tosaka M, Murakami S, Poompradub S, Kohjiya S, Ikeda Y, Toki S, et al. Orientation and crystallization of natural rubber network as revealed by WAXD using synchrotron radiation. Macromolecules. 2004;37:3299-309. http://dx.doi.org/10.1021/ma0355608.

18. Toki S, Sics I, Ran S, Liu L, Hsiao BS, Murakami S, et al. Strain-induced molecular orientation and crystallization in natural and synthetic rubbers under uniaxial deformation by in-situ synchrotron X-ray study. Rubber Chem Technol. 2004;77:317-35. http://dx.doi.org/10.5254/1.3547826.

19. Imbernon L, Pauchet R, Pire M, Albouy PA, Tencé-Girault S, Norvez S. Strain-induced crystallization in sustainably crosslinked epoxidized natural rubber. Polymer (Guildf). 2016;93:189-97. http://dx.doi.org/10.1016/j.polymer.2016.04.023.

20. Poompradub S, Tosaka M, Kohjiya S, Ikeda Y, Toki S, Sics I, et al. Mechanism of strain-induced crystallization in filled and unfilled natural rubber vulcanizates. J Appl Phys. 2005;97:103529. http://dx.doi.org/10.1063/1.1900927.

21. Chenal JM, Gauthier C, Chazeau L, Guy L, Bomal Y. Parameters governing strain induced crystallization in filled natural rubber. Polymer (Guildf). 2007;48:6893-901. http://dx.doi.org/10.1016/j.polymer.2007.09.023.

22. Waesateh K, Saiwari S, Ismail H, Othman N, Soontaranon S, Hayeemasae N. Features of crystallization behavior of natural rubber/halloysite nanotubes composites using synchrotron wide-angle X-ray scattering. Int J Polym Anal Charact. 2018;23:260-70. http://dx.doi.org/10.1080/1023666X.2018.1438773.

23. ASTM: American Society for Testing and Materials. ASTM D5289: Standard Test Method for Rubber Property-Vulcanization Using Rotorless Cure Meters. West Conshohocken: ASTM; 2019.

24. ASTM: American Society for Testing and Materials. ASTM D412: Standard Test Methods for Vulcanized Rubber and Thermoplastic Elastomers-Tension. West Conshohocken: ASTM; 2021.

25. ASTM: American Society for Testing and Materials. ASTM D624: Standard Test Method for Tear Strength of Conventional Vulcanized Rubber and Thermoplastic Elastomers. West Conshohocken: ASTM; 2020.

26. ASTM: American Society for Testing and Materials. ASTM D2240: Standard Test Method for Rubber Property-Durometer Hardness. West Conshohocken: ASTM; 2021.

27. Marykutty C, Mathew G, Mathew E, Thomas S. Studies on novel binary accelerator system in sulfur vulcanization of natural rubber. J Appl Polym Sci. 2003;90:3173-82. http://dx.doi.org/10.1002/app.13023.

28. Osaka N, Kato M, Saito H. Mechanical properties and network structure of phenol resin crosslinked hydrogenated acrylonitrile-butadiene rubber. J Appl Polym Sci. 2013;129:3396-403. http://dx.doi.org/10.1002/app.39010.

29. Li S, Xu T, Jia Z, Zhong B, Luo Y, Jia D, et al. Preparation and stress-strain behavior of in-situ epoxidized natural rubber/SiO$_2$ hybrid through a sol-gel method. Express Polym Lett. 2018;12:180-5. http://dx.doi.org/10.3144/expresspolymlett.2018.16.

Insight into Mechanical Properties and Strain-induced Crystallisation of Epoxidized Natural Rubber Filled
with Various Silanized Halloysite Nanotubes

11

30. Kadi S, Lellou S, Marouf-Khelifa K, Schott J, Gener-Batonneau I, Khelifa A. Preparation, characterisation and application of thermally treated Algerian halloysite. Microporous Mesoporous Mater. 2012;158:47-54. http://dx.doi.org/10.1016/j.micromeso.2012.03.014.

31. Rooj S, Das A, Thakur V, Mahaling R, Bhowmick AK, Heinrich G. Preparation and properties of natural nanocomposites based on natural rubber and naturally occurring halloysite nanotubes. Mater Des. 2010;31:2151-6. http://dx.doi.org/10.1016/j.matdes.2009.11.009.

32. Ismail H, Pasbakhsh P, Ahmad Fauzi M, Abu Bakar A. The effect of halloysite nanotubes as a novel nanofiller on curing behaviour, mechanical and microstructural properties of ethylene propylene diene monomer (EPDM) nanocomposites. Polym Plast Technol Eng. 2009;48:313-23. http://dx.doi.org/10.1080/03602550802675736.

33. Kaewsakul W, Sahakaro K, Dierkes WK, Noordermeer JWM. Mechanistic aspects of silane coupling agents with different functionalities on reinforcement of silica-filled natural rubber compounds. Polym Eng Sci. 2015;55:836-42. http://dx.doi.org/10.1002/pen.23949.

34. Nun-anan P, Wisunthorn S, Pichaiyut S, Nathaworn CD, Nakason C. Influence of nonrubber components on properties of unvulcanized natural rubber. Polym Adv Technol. 2020;31:44-59. http://dx.doi.org/10.1002/pat.4746.

35. Hayeemasae N, Sensem Z, Surya I, Sahakaro K, Ismail H. Synergistic effect of maleated natural rubber and modified palm stearin as dual compatibilizers in composites based on natural rubber and halloysite nanotubes. Polymers (Basel). 2020;12:766. http://dx.doi.org/10.3390/polym12040766.

36. Hayeemasae N, Sensem Z, Sahakaro K, Ismail H. Maleated natural rubber/halloysite nanotubes composites. Processes (Basel). 2020;8:286. http://dx.doi.org/10.3390/pr8030286.

37. Ozbas B, Toki S, Hsiao BS, Chu B, Register RA, Aksay IA, et al. Strain-induced crystallization and mechanical properties of functionalized graphene sheet-filled natural rubber. J Polym Sci, B, Polym Phys. 2012;50:718-23. http://dx.doi.org/10.1002/polb.23060.

38. Candau N, Oguz O, Federico CE, Stoclet G, Tahon JF, Maspoch ML. Strain induced crystallization in vulcanized natural rubber containing ground tire rubber particles with reinforcement and nucleation abilities. Polym Test. 2021;101:107313. http://dx.doi.org/10.1016/j.polymertesting.2021.107313.

39. Kuang W, Yang Z, Tang Z, Guo B. Wrapping of polyrhodanine onto tubular clay and its prominent effects on the reinforcement of the clay for rubber. Compos, Part A Appl Sci Manuf. 2016;84:344-53. http://dx.doi.org/10.1016/j.compositesa.2016.02.015.